Effects of an isovector scalar meson on the equation of state of dense matter within a relativistic mean field model

Virender Thakur,[1,*] Raj Kumar,[1,†] Pankaj Kumar,[2] Vikesh Kumar,[1] Mukul Kumar,[1] C. Mondal,[3,‡] B. K. Agrawal,[4,§] and Shashi K. Dhiman[1,5,‖]

[1]*Department of Physics, Himachal Pradesh University, Shimla 171005, India*
[2]*Department of Applied Sciences, CGC College of Engineering, Landran, Mohali 140307, India*
[3]*Laboratoire de Physique Corpusculaire, CNRS, ENSICAEN, UMR6534, Université de Caen Normandie, F-14000, Caen Cedex, France*
[4]*Saha Institute of Nuclear Physics, 1/AF Bidhannagar, Kolkata 700064, India*
[5]*School of Applied Sciences, Himachal Pradesh Technical University, Hamirpur 177001, India*

(Received 3 May 2022; revised 4 August 2022; accepted 28 September 2022; published 18 October 2022)

The effects of the isovector scalar δ-meson field on the properties of finite nuclei, infinite nuclear matter, and neutron stars are investigated within a relativistic mean field (RMF) model which includes nonlinear couplings. Several parameter sets (SRVs) are generated to asses the influence of the δ meson on the properties of neutron stars. These parametrizations correspond to different values of the coupling constant of the δ meson to nucleons, with remaining ones calibrated to yield finite nuclei and infinite nuclear matter properties consistent with the available experimental data. It is observed that, to fit the properties of finite nuclei and infinite nuclear matter, a stronger coupling between the isovector vector ρ meson and nucleons is required in the presence of a δ field. Furthermore, the δ meson is found to affect the radius of the canonical neutron star significantly. The value of dimensionless tidal deformability, Λ, for the canonical neutron star also satisfies the constraints from the waveform model analysis of the GW170817 binary neutron star merger event. A covariance analysis is performed to estimate the statistical uncertainties of the model parameters as well as correlations among the model parameters and different observables of interest.

DOI: 10.1103/PhysRevC.106.045806

I. INTRODUCTION

Neutron stars are the densest objects in the observable universe and deep knowledge of the equation of state (EoS) of dense matter in beta equilibrium is thus required to understand their behavior. It has been shown that the dense matter EoS must be treated relativistically [1,2]. For this reason, relativistic mean field (RMF) models have been widely used to obtain a realistic description of the properties of finite nuclei, bulk nuclear matter, and neutron stars. Currently, many different variants of RMF models with various couplings are in use to study finite nuclei and neutron star properties [3–5]. Accurate constraints are necessary to understand the limits of these different types of models. During the last decade, a wide range of astrophysical observations—such as the precise measurement of massive millisecond pulsars using the Shapiro delay technique [6,7], detection of gravitational waves generated by binary neutron stars in the GW170817 event by the LIGO-Virgo Collaboration [8,9], and the joint mass radius measurement of neutron stars using the x-ray timing technique by the NICER Collaboration [10–13]—have started to provide unprecedented new constraints on the dense matter EoS. They have triggered plethora of theoretical studies to look at the dense matter EoS from very different perspectives; see Ref. [14] and references therein. First-of-its-kind model independent measurement of neutron skin thickness Δr_{np} of ^{208}Pb [15] and ^{48}Ca [16] at the Jefferesen laboratory also inspired theoretical studies to take a fresher look at the isovector channel of the nuclear interaction [17–21].

The effective mass of a nucleon quantifies the momentum dependence of the nuclear force in the medium. It can be quoted for infinite nuclear matter at the Fermi surface. It is, however, necessary to realize that the concept of effective mass is different in nonrelativistic [22,23] and relativistic formalisms [24]. Nevertheless, it plays some crucial roles in determining various finite nuclear properties, e.g., isoscalar giant quadrupole resonance (ISGQR) [25] and nucleon nucleon scattering in optical potentials [26], or even in realizing various properties of nuclear matter and neutron stars [27,28]. Recently, a systematic study was performed using RMF models which assessed the impact of relativistic (Dirac) effective mass (M^*) on the properties of neutron stars [29]. The isovector splitting of the effective mass, which measures the difference between neutron (M_n^*) and proton (M_p^*) effective mass, can also influence greatly the physical properties of finite nuclei, such as locating the drip lines [30] or nucleon-nucleus scattering of asymmetric systems [26]. Its impact increases manifold in high density environments

*virenthakur2154@gmail.com
†raj.phy@gmail.com
‡mondal@lpccaen.in2p3.fr
§sinp.bijay@gmail.com
‖shashi.dhiman@gmail.com

which can alter thermal and transport properties of asymmetric matter [31,32] or neutrino opacities of neutron star matter [33]. To settle its value, even at saturation, remains a persisting challenge both theoretically [34–38] and experimentally [26,39,40].

Appearance of isovector splitting of effective mass to the leading order in RMF models occurs through the isovector scalar δ mesons. It impacts the proton fraction in neutron stars and hence the cooling process of neutron stars after formation [41,42]. It can also influence the global properties of neutron stars [27,28,43–46]. A systematic study of RMF models with added freedom in the isospin channel through the δ meson, optimized using well constrained finite nuclear properties and extrapolating at high density to understand the properties of neutron stars and in general the dense matter EoS, can enhance our knowledge of the density dependence of the isovector channel of nuclear interaction.

The present study is aimed towards investigating the effects of the δ meson on the dense matter EoS within the framework of RMF model. We generate several parameter sets by varying the coupling strength of the δ meson to nucleons such that the low density behavior of the EoSs remain consistent with the available finite nuclei data and a few empirical properties of infinite nuclear matter evaluated at the saturation density. The properties of neutron stars obtained with these EoSs are them compared to assess the role of δ mesons.

The paper is organized as follows. In Sec. II, the theoretical framework which is used to construct the EoS for neutron stars is discussed. We also discuss the procedure to optimize the coupling constants and the method to perform a covariance analysis in the same section. In Sec. III, we present our results. We summarize and draw our conclusions in Sec. IV.

II. FORMALISM

A. Theoretical model

The Lagrangian density for the RMF model used in the present study—based on different nonlinear self-couplings and intercouplings among isoscalar scalar σ, isoscalar vector ω_μ, isovector scalar δ, and isovector vector ρ_μ meson fields and the nucleonic Dirac field Ψ [47,48] is given by,

$$\begin{aligned}\mathcal{L} = \sum_q \overline{\Psi}\Big[i\gamma^\mu\partial_\mu - (M - g_\sigma\sigma - g_\delta\delta\cdot\tau) - \Big(g_\omega\gamma^\mu\omega_\mu \\ + \frac{1}{2}g_\rho\gamma^\mu\tau\cdot\rho_\mu\Big)\Big]\Psi + \frac{1}{2}\big(\partial_\mu\sigma\,\partial^\mu\sigma - m_\sigma^2\sigma^2\big) \\ - \frac{\overline{\kappa}}{3!}g_\sigma^3\sigma^3 - \frac{\overline{\lambda}}{4!}g_\sigma^4\sigma^4 - \frac{1}{4}\omega_{\mu\nu}\omega^{\mu\nu} + \frac{1}{2}m_\omega^2\omega_\mu\omega^\mu \\ + \frac{1}{4!}\zeta\, g_\omega^4(\omega_\mu\omega^\mu)^2 - \frac{1}{4}\rho_{\mu\nu}\rho^{\mu\nu} + \frac{1}{2}m_\rho^2\rho_\mu\rho^\mu \\ + \frac{1}{2}\big(\partial_\mu\delta\partial^\mu\delta - m_\delta^2\delta^2\big) + \frac{1}{2}c_1 g_\omega^2 g_\rho^2\omega_\mu\omega^\mu\rho_\mu\rho^\mu. \qquad (1)\end{aligned}$$

The Dirac effective mass for the nucleons (q) appearing in the Lagrangian density above is specified as

$$M_q^* = (M - g_\sigma\sigma - g_\delta\delta\cdot\tau), \qquad (2)$$

where $\tau = 1$ (-1) for $q =$ neutron (proton). Following the Euler-Lagrange formalism one can readily find the expressions for energy density $\mathcal{E}$ and pressure P as a function of density from Eq. (1) [49].

B. Optimization and covariance analysis

In the present study, five new relativistic interactions SRV00, SRV01, SRV02, SRV03, and SRV04 have been generated for the Lagrangian density given by Eq. (1) to investigate the effect of δ mesons on the properties of finite nuclei and neutron star matter. Here, SRV00, SRV01, SRV02, SRV03, and SRV04 parametrizations correspond to different values of the coupling of the δ meson to the nucleon, i.e., $g_\delta = 0.0$, 1.0, 2.0, 3.0, and 4.0 respectively. As the effect of the δ meson is predominantly important at suprasaturation densities, one can *a priori* anticipate its insignificant impact in finite nuclei, which is primarily sensitive to the EoS at subsaturation densities. This is the reason why we kept fixed the g_δ at aforementioned values, optimizing the rest of the parameters in Eq. (1). This is not far from the strategy recently used by Li *et al.* in Ref. [46]. The parameters of the model are obtained by fitting the experimental data [50] on binding energies (BEs) and charge rms radii (r_{ch}) [51] of some spherical nuclei, ^{16,24}O, ^{40,48}Ca, ^{56,78}Ni, ^{88}Sr, ^{90}Zr, ^{100,116,132}Sn, and ^{208}Pb. For the open shell nuclei, the pairing has been included using the BCS formalism with constant pairing gaps [52,53] that are taken from the nucleon separation energies of neighboring nuclei [50]. Neutron and proton pairing gaps are evaluated by using fourth-order finite difference mass formula (five point difference) [54]. The neutron and proton pairing gaps (Δ_n, Δ_p) in MeV for the open shell nuclei are ^{88}Sr(0.0,1.284), ^{90}Zr(0.0,1.239), and ^{116}Sn(1.189,0.0). The neutron pairing gap for ^{24}O practically vanishes since the first unoccupied orbit $1d_{3/2}$ is almost 4.5 MeV above the completely filled $2s_{1/2}$ orbit [55,56]. The pairing correlation energies for a fixed gap Δ is calculated by using the pairing window of $2\hbar\omega$, where $\hbar\omega = 45A^{-1/3}$–$25A^{-2/3}$ MeV [48]. We also incorporated the recently measured neutron skin thickness of ^{208}Pb using the parity violating electron scattering experiment [15] in our fit data. The optimization of the parameters ($\mathbf{p}$) appearing in the Lagrangian [Eq. (1)] is done by using the simulated annealing method (SAM) [57–59] by following a χ^2 minimization procedure which is given as

$$\chi^2(\mathbf{p}) = \frac{1}{N_d - N_p}\sum_{i=1}^{N_d}\left(\frac{M_i^{\rm exp} - M_i^{\rm th}}{\sigma_i}\right)^2, \qquad (3)$$

where N_d is the number of experimental data points and N_p is the number of fitted parameters. The σ_i denotes adopted errors [60,61] and $M_i^{\rm exp}$ and $M_i^{\rm th}$ are the experimental and the corresponding theoretical values, respectively, for a given observable. The minimum value of χ_0^2 corresponds to the optimal values $\mathbf{p}_0$ of the parameters.

Once the optimized parameter set is obtained, the correlation coefficient between two quantities Y and Z can be

TABLE I. SRV parameter sets for the Lagrangian of RMF model as given in Eq. (1). The parameter $\overline{\kappa}$ is in fm^{-1}. The values of meson masses m_σ, m_ω, m_ρ, and m_δ are in MeV. The nucleonic mass (M) and meson masses (m_ω, m_ρ, and m_δ) are taken as 939, 782.5, 762.468, and 980 MeV, respectively. The values of $\overline{\kappa}$, $\overline{\lambda}$, and c_1 are multiplied by 10^2.

Parameter	SRV00	SRV01	SRV02	SRV03	SRV04
g_σ	10.3109 ± 0.1109	10.3442 ± 0.0978	10.3344 ± 0.1135	10.3723 ± 0.0999	10.3735 ± 0.1294
g_ω	13.1772 ± 0.1621	13.2508 ± 0.1379	13.2137 ± 0.1414	13.3113 ± 0.1269	13.2984 ± 0.1815
g_ρ	10.8834 ± 1.1730	11.2832 ± 1.0110	11.5834 ± 0.9676	12.4834 ± 1.1274	13.1833 ± 0.8043
$\overline{\kappa}$	1.8509 ± 0.0500	1.8624 ± 0.0700	1.8780 ± 0.0200	1.8242 ± 0.0500	1.8490 ± 0.0800
$\overline{\lambda}$	−0.05151 ± 0.0700	−0.05803 ± 0.0600	−0.06060 ± 0.0600	−0.04934 ± 0.0800	−0.05621 ± 0.0800
ζ	0.02116 ± 0.0017	0.02050 ± 0.0013	0.02017 ± 0.0011	0.02177 ± 0.0012	0.02089 ± 0.0027
c_1	4.60038 ± 2.3600	4.49219 ± 1.9200	4.20853 ± 1.5600	3.66169 ± 1.4900	3.01068 ± 0.8800
m_σ	501.9596 ± 0.9230	501.0200 ± 1.0071	501.6638 ± 1.3141	500.7480 ± 1.2629	501.0215 ± 1.3663

calculated by covariance analysis [60–64] as

$$r_{YZ} = \frac{\overline{\Delta Y\,\Delta Z}}{\sqrt{\overline{\Delta Y^2}\;\;\overline{\Delta Z^2}}}, \tag{4}$$

where covariance between Y and Z is expressed as

$$\overline{\Delta Y\,\Delta Z} = \sum_{\alpha\beta}\left(\frac{\partial Y}{\partial p_\alpha}\right)_{\mathbf{p}_0} C^{-1}_{\alpha\beta}\left(\frac{\partial Z}{\partial p_\beta}\right)_{\mathbf{p}_0}. \tag{5}$$

Here, $C^{-1}_{\alpha\beta}$ is an element of inverted curvature matrix given by

$$C_{\alpha\beta} = \frac{1}{2}\left(\frac{\partial^2\chi^2(\mathbf{p})}{\partial p_\alpha \partial p_\beta}\right)_{\mathbf{p}_0}. \tag{6}$$

The standard deviation, $\overline{\Delta Y^2}$, in Y can be computed using Eq. (5) by substituting $Z = Y$.

III. RESULTS AND DISCUSSION

We have obtained five different parameter sets corresponding to different values of g_δ by calibrating the remaining parameters to a suitable set of finite nuclei as described earlier. All parametrizations obtained in the present work give equally good fit to the properties of finite nuclei which were used for the optimization procedure. In Table I we display optimum values of the model parameters for all five SRV parameter sets along with the uncertainties on them computed using Eq. (5). It can be seen that the parameter g_ρ increases with the increase in value of g_δ. A larger value of g_ρ is required in the presence of the δ field to fit the properties of finite nuclei. As the contribution of the δ field is attractive, increased binding due to the δ field has to be compensated by the higher value of the repulsion by the ρ field. The parameter g_ρ has its lowest value for the SRV00 parametrization ($g_\delta = 0$). For any finite value of δ coupling ($g_\delta > 0$), i.e., for SRV01, SRV02, SRV03, and SRV04 parametrizations, the strength of ρ coupling (g_ρ) increases gradually. The cross-coupling between the ω_μ and ρ_μ fields quantified by the term c_1 decreases slightly from 4.6003 to 3.0107 as the value of coupling constant g_δ increases from 0.0 to 4.0 corresponding to different SRV parametrizations.

In Table II, different observables fitted in the present work, their experimental values [50,51], adopted errors σ on them [65], along with the calculated values for different SRV parametrizations are displayed. The estimated uncertainties are also listed for the fitted observables. The fitted values of finite nuclei properties are quite close to their experimental counterparts. The root mean square (rms) errors on the BEs are found to be in the range 1.50–1.86 MeV, and the ones for r_{ch} are found to be 0.02 fm for the different parametrizations. It is quite interesting to observe that, even though g_δ influences the coupling g_ρ, the isovector sensitive observable Δr_{np} varies only slightly, ≈0.01 fm, across the different SRV models obtained in the present work. This observation is quite similar to the one obtained by Li *et al.* [46]. In Table III, we present the results for the properties of symmetric nuclear matter (SNM) such as binding energy per nucleon (E/A), incompressibility (K), the ratio of effective mass to the mass of nucleon (M^*/M), along with the symmetry energy coefficient (J), and its slope (L), all are evaluated at the saturation density (ρ_0). We also quote the theoretically calculated error on them. The results are presented for all five SRV parametrizations. The value of E/A lies in the range −16.09 to −16.12 for the five parametrizations. The values of J and L obtained by our parametrizations are consistent with the constraints from observational analysis, $J = 31.6 \pm 2.66$ MeV and $L = 58.9 \pm 16$ MeV [66,67]. The value of K is also in agreement with the value 240 ± 20 MeV determined from the isoscalar giant monopole resonance (ISGMR) for ^{90}Zr and ^{208}Pb nuclei [68,69]. It can also be seen from Table III that the mean values of the slope of symmetry energy (L) for SRV parametrizations decrease with the increase in the value of g_δ. The average value of L decreases from 65.23 MeV in SRV00 to 55.31 MeV for SRV04. It can be noted that the isoscalar properties (E/A, K, ρ_0, and M^*/M) are well constrained for all SRV parametrizations. The only exception is the error on K in the case of SRV04, where the error is almost 10% of its central value. But in the isovector sector, the percentage error on the slope of symmetry energy (L) are consistently on the larger side for all SRV parametrizations.

The importance of performing covariance analysis in theoretical studies was pointed out recently [60,63]. It not only enables one to quote statistical uncertainties on model parameters or any calculated observables, but also provides complementary information about the sensitivity of the parameters to physical observables, redundancies among fitted observables, or interdependencies among model parameters. As our primary objective is not to establish an ultimate model,

TABLE II. The values of binding energy (BE) and charge radii (r_{ch}) of fitted nuclei along with theoretical errors obtained for different SRV parametrizations. The corresponding experimental values [50,51] are also listed. The value of neutron skin thickness (Δr_{np}) for ^{208}Pb is given along with the experimental data [15]. The adopted errors on the observables (σ) used for optimization of parameters are also displayed. The values of BE are given in units of MeV and r_{ch} and Δr_{np} are in fm.

Nucleus	Observables	Expt.	σ	SRV00	SRV01	SRV02	SRV03	SRV04
^{16}O	BE	127.62	4.0	128.67 ± 0.52	128.83 ± 0.50	128.94 ± 0.55	128.90 ± 0.51	128.94 ± 0.61
	r_{ch}	2.699	0.04	2.709 ± 0.008	2.712 ± 0.023	2.711 ± 0.031	2.710 ± 0.013	2.710 ± 0.023
^{24}O	BE	168.96	1.0	169.95 ± 0.96	169.38 ± 0.90	169.64 ± 0.89	168.90 ± 1.01	169.00 ± 0.93
^{40}Ca	BE	342.04	3.0	343.40 ± 0.69	343.14 ± 0.65	343.18 ± 0.53	344.41 ± 0.63	344.39 ± 0.91
	r_{ch}	3.478	0.02	3.454 ± 0.014	3.457 ± 0.007	3.455 ± 0.016	3.455 ± 0.014	3.455 ± 0.017
^{48}Ca	BE	415.97	1.0	415.59 ± 0.54	415.15 ± 0.52	415.37 ± 0.45	415.37 ± 0.63	415.48 ± 0.52
	r_{ch}	3.477	0.02	3.468 ± 0.016	3.469 ± 0.014	3.468 ± 0.014	3.467 ± 0.014	3.467 ± 0.022
^{56}Ni	BE	484.01	5.0	482.05 ± 1.28	482.39 ± 1.21	482.28 ± 1.31	483.12 ± 1.48	483.22 ± 1.56
	r_{ch}	3.750	0.02	3.712 ± 0.022	3.709 ± 0.017	3.708 ± 0.14	3.707 ± 0.017	3.705 ± 0.013
^{78}Ni	BE	642.56	2.0	641.39 ± 1.03	640.01 ± 0.97	641.05 ± 1.01	640.21 ± 1.08	640.18 ± 1.07
^{88}Sr	BE	768.42	1.0	768.24 ± 0.60	767.72 ± 0.57	767.84 ± 0.58	768.39 ± 0.60	768.40 ± 0.62
	r_{ch}	4.219	0.02	4.226 ± 0.016	4.227 ± 0.014	4.227 ± 0.013	4.225 ± 0.021	4.225 ± 0.0146
^{90}Zr	BE	783.81	1.0	783.92 ± 0.69	783.58 ± 0.64	783.59 ± 0.68	784.37 ± 0.69	784.36 ± 0.68
	r_{ch}	4.269	0.02	4.280 ± 0.019	4.280 ± 0.019	4.280 ± 0.013	4.278 ± 0.029	4.278 ± 0.015
^{100}Sn	BE	825.10	2.0	826.60 ± 1.28	826.95 ± 1.24	827.56 ± 1.14	827.09 ± 1.23	827.01 ± 1.66
^{116}Sn	BE	988.67	2.0	988.34 ± 0.83	987.74 ± 0.73	987.72 ± 2.18	988.49 ± 0.82	988.25 ± 0.88
	r_{ch}	4.627	0.02	4.617 ± 0.016	4.618 ± 0.014	4.617 ± 0.009	4.615 ± 0.012	4.615 ± 0.020
^{132}Sn	BE	1100.22	1.0	1101.38 ± 0.84	1100.58 ± 0.80	1101.48 ± 0.77	1100.59 ± 0.86	1100.70 ± 0.82
	r_{ch}	4.709	0.02	4.721 ± 0.019	4.721 ± 0.019	4.720 ± 0.010	4.719 ± 0.012	4.717 ± 0.011
^{208}Pb	BE	1636.34	1.0	1636.58 ± 1.03	1635.98 ± 0.98	1636.32 ± 0.96	1636.27 ± 1.05	1636.10 ± 1.02
	r_{ch}	5.501	0.02	5.530 ± 0.015	5.531 ± 0.014	5.529 ± 0.014	5.527 ± 0.021	5.526 ± 0.011
	Δr_{np}	0.283 ± 0.071	0.071	0.222 ± 0.032	0.223 ± 0.028	0.217 ± 0.026	0.215 ± 0.035	0.214 ± 0.029

for the purpose of demonstration we will discuss the results of covariance analysis as outlined in Sec. II B, only for the model SRV02. The results for other parameter sets are quite similar (not shown here). In Fig. 1, the correlation coefficients between different model parameters appearing in Eq. (1) are outlined for SRV02 parametrization. A strong correlation is found between several pairs of model parameters, such as g_σ and g_ω, g_ρ and c_1, and $\bar{\lambda}$ and ζ with correlation coefficients 0.99, 0.98, and 0.95, respectively. These interdependencies mean that, if one of these pairs are fixed at a particular value, the other must attain the precise value as suggested by their correlation to satisfactorily obtain the fit data. The results obtained for the correlations among model parameters presented in Fig. 1 are quite similar to those obtained in Refs. [19,70]. The strong correlation between L and Δr_{np}, which is shown later (see Fig. 3), may be attributed to the large experimental error on Δr_{np} for ^{208}Pb, which also led us to choose a rather large adopted error during optimization. The theoretical errors on the Δr_{np} of the ^{208}Pb nucleus are found to be 0.032, 0.028, 0.026, 0.0353, and 0.029 fm for SRV00, SRV01, SRV02, SRV03, and SRV04 parametrizations, respectively. These are much smaller compared to the adopted error (0.071 fm, which is also the experimental error obtained in Ref. [15]).

We now display in Fig. 2 the correlation coefficients between the model parameters appearing in the Lagrangian [Eq. (1)] and the different properties of interest corresponding to SNM and the neutron skin thickness Δr_{np} of ^{208}Pb for SRV02. A strong correlation is observed between the isovector parameter g_ρ with the symmetry energy coefficient (J), its slope (L), and Δr_{np} of ^{208}Pb. The vector mixing parameter c_1 is also found to have a strong correlation with J and L. This strong correlation is anticipated, as c_1 and g_ρ are strongly correlated

TABLE III. The bulk nuclear matter properties at saturation density for SRV parametrizations are listed: ρ_0, E/A, K, J, L, and M^*/M denote the saturation density, binding energy per nucleon, incompressibility coefficient, symmetry energy, the slope of symmetry energy, and the ratio of effective nucleon mass to the nucleon mass, respectively.

Parameter	SRV00	SRV01	SRV02	SRV03	SRV04
ρ_0 (fm^{-3})	0.149 ± 0.003	0.149 ± 0.002	0.149 ± 0.002	0.149 ± 0.003	0.149 ± 0.008
E/A (MeV)	−16.11 ± 0.06	−16.11 ± 0.05	−16.09 ± 0.05	−16.12 ± 0.06	−16.11 ± 0.04
K (MeV)	223.94 ± 8.57	221.78 ± 9.95	222.05 ± 5.47	221.72 ± 10.62	221.11 ± 23.20
J (MeV)	33.49 ± 1.82	33.75 ± 1.77	33.31 ± 1.78	33.54 ± 2.13	33.34 ± 2.08
L (MeV)	65.23 ± 15.37	63.82 ± 13.50	61.49 ± 13.22	58.06 ± 15.93	55.31 ± 13.76
M^*/M	0.606 ± 0.013	0.602 ± 0.010	0.603 ± 0.005	0.601 ± 0.009	0.600 ± 0.009

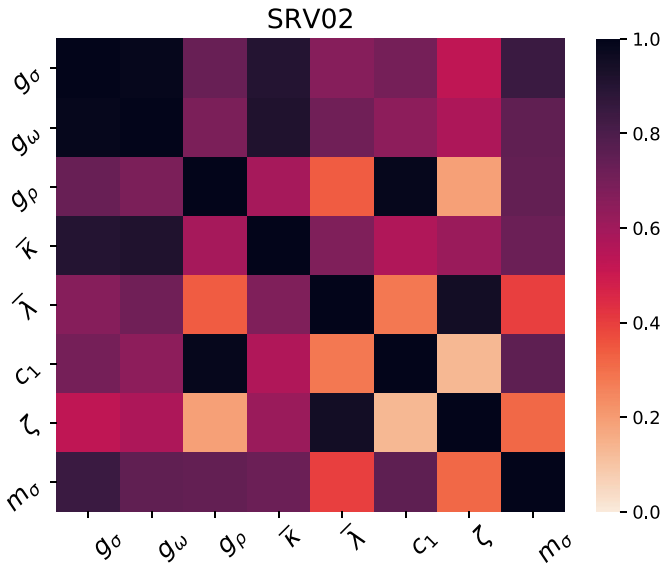

FIG. 1. Correlation coefficients (absolute values) among the model parameters for SRV02 parametrization for the Lagrangian given by Eq. (1).

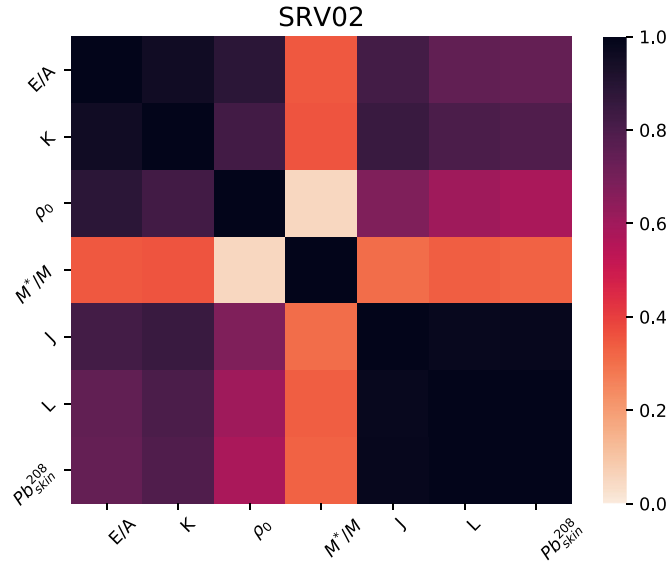

FIG. 3. Correlation coefficients (absolute values) for a few bulk nuclear matter properties and the neutron skin of ^{208}Pb for SRV02 parametrization.

to each other, which was observed in Fig. 1. It is also realized from Fig. 2 that bulk properties of SNM like E/A, K, ρ_0, and M^*/M have strong correlations with isoscalar coupling parameters g_σ, g_ω, and $\bar{\kappa}$. This study is quite consistent with previous calculations in the literature [20,56,70]. In Fig. 3, we display the correlation coefficients among the different observables in graphical form, particularly those which were also shown in Fig. 2. In the isoscalar sector the only strong correlation observed is between binding energy per nucleon (E/A) and incompressibility coefficient (K). K also shows some mild correlations with all other observables displayed

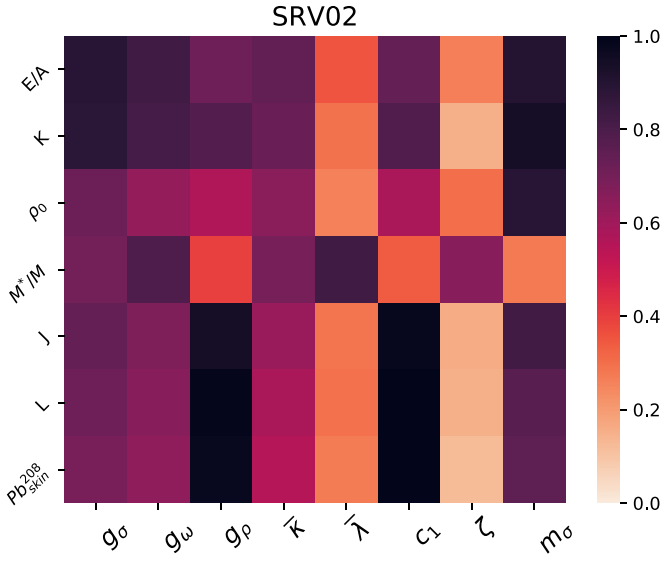

FIG. 2. Correlation coefficients (absolute values) between the model parameters and a set of physical observables for the SRV02 parametrization (see text for details).

in the figure. The symmetry energy J and its slope parameter L are found to be strongly correlated. As mentioned earlier in the discussion of Table III, we observe a strong correlation of the neutron skin thickness of ^{208}Pb with J and L. These results are also in line with earlier ones [70].

It is quite important to emphasize that we kept fixed the strength of the coupling of the δ meson at different values and optimized the rest. This might be partially responsible for imparting a strong correlation among the isovector sensitive parameters g_ρ, c_1 to J, L, or Δr_{np} of ^{208}Pb (see Fig. 2) in reproducing the fitted data within bounds. It gets further clarified in the strong correlations among Δr_{np} (^{208}Pb), J, and L in Fig. 3. Anticipating the results obtained for neutron stars which are discussed later, this strong correlation somewhat restricts the behavior of the matter at high densities in the isovector channel, resulting in a monotonic increase in the radius and tidal deformability of a $1.4M_\odot$ neutron star (see Table IV) with the increase of the δ meson coupling g_δ. A full optimization is thus needed with suitable data in the future, including g_δ, to understand this behavior further. To study the effects of the δ meson on nucleon mass, in Fig. 4 the effective masses of the proton and neutron are plotted as a function of baryon density for three values of asymmetry parameter $\alpha = 0, 0.5, 1$ ($\alpha = \frac{\rho_n - \rho_p}{\rho_n + \rho_p}$) for the SRV04 parametrization, which has the largest value of g_δ among all SRV variants obtained in the present work. The asymmetry parameter $\alpha = 0.0$ represents SNM and $\alpha = 1$ corresponds to pure neutron matter (PNM). It is clear from Eq. (2) that the presence of the δ meson leads to splitting of the nucleon mass. For SNM, there is no splitting of the nucleon mass. In Fig. 4, the solid (dashed) lines depict the effective mass of the proton (neutron) for $\alpha = 0$, 0.5, and 1.0. One can observe from the figure that the effective proton mass is larger than the neutron effective mass. The splitting of the proton and neutron effective masses due to the δ meson can be important in a

TABLE IV. The properties of a nonrotating neutron star for the various EoSs computed with SRV parameter sets are presented along with the theoretical errors on them. M_G and R_{max} denote the Maximum Gravitational mass and corresponding radius. The values for $R_{1.4}$ and $\Lambda_{1.4}$ denote radius and dimensionless tidal deformability at $1.4M_\odot$.

No.	EoS	M_G ($M_\odot$)	R_{max} (km)	$R_{1.4}$ (km)	$R_{2.0}$ (km)	$\Lambda_{1.4}$
1.	SRV00	2.04 ± 0.03	11.48 ± 0.08	12.92 ± 0.22	12.07 ± 0.31	484.16 ± 62.10
2.	SRV01	2.06 ± 0.02	11.55 ± 0.13	12.99 ± 0.20	12.24 ± 0.21	504.95 ± 58.02
3.	SRV02	2.07 ± 0.02	11.67 ± 0.07	13.16 ± 0.13	12.43 ± 0.14	565.52 ± 60.33
4.	SRV03	2.08 ± 0.02	11.81 ± 0.11	13.41 ± 0.21	12.60 ± 0.16	652.60 ± 52.01
5.	SRV04	2.13 ± 0.06	12.11 ± 0.23	13.86 ± 0.21	13.09 ± 0.33	783.96 ± 70.03

highly asymmetric system like a neutron star or supernova environment. At the center of a neutron star the density can reach ≈5–6 ρ_0 and $\alpha \approx 0.7$–0.8. One can readily estimate the amount of splitting in the effective mass in this situation by looking at Fig. 4. It can also affect the transport properties of neutron star matter [74].

To assess the impact of the δ meson on the global properties of neutron stars, we plot the gravitational mass (M_G) of a nonrotating neutron star as a function of radius for all SRV parametrizations in Fig. 5. The maximum mass (M_{max}) and the corresponding radius (R_{max}) of a neutron star for all the models obtained here lie in the range 2.04–2.13 $M_\odot$ and 11.48–12.11 km, respectively. This satisfies the recently measured radius of PSRJ0740+6620 of $12.45^{+0.65}_{-0.65}$ km by the NICER Collaboration [12,13]. The radius of a neutron star of $2M_\odot$ is also in accordance with the observational data of PSRJ0740+6620 by NICER [12,13]. The maximum mass of a neutron star attained by various SRV parametrizations supports the constraint from PSRJ0740+6620 with the mass of $2.08 \pm 0.07 M_\odot$ [75,76]. It is observed that the radius ($R_{1.4}$) of a neutron star with mass $1.4M_\odot$, can be significantly affected by the presence of δ mesons as we move from parametrization set SRV00 to SRV04. The value of $R_{1.4}$ with the inclusion of the TM1 crust EoS [77] lies in the range 12.92–13.86 km, which is also in line with the range proposed in Ref. [12,78]. It is observed that the radius $R_{1.4}$ increases by 7.27% and the maximum mass of neutron star changes by 4.4% from SRV00 to SRV04 parametrizations with the variation of coupling $g_\delta = 0.0$ to 4.0. This change in the neutron star properties may be attributed to the impact of the δ meson, which affects high-density behavior of asymmetric nuclear matter.

Tidal deformability imparted by companion stars on one another in a binary system can yield remarkable information on the EoS for neutron stars [79,80]. In Fig. 6, we show the results of dimensionless tidal deformability Λ, defined as $\Lambda = (2/3)k_2(R/M_G)^5$, where k_2 is the Love number, as a function of the neutron star mass M_G for different SRV models. The recent constraints on the tidal deformability $\Lambda_{1.4}$ of a $1.4M_\odot$ neutron star including GW170817 [8,81] is also given in the figure. The value of $\Lambda_{1.4}$ lies in the range 484–783 for different SRV parametrizations, which satisfies the proposed limit as listed in Refs. [8,78,81,82]. The value of $\Lambda_{1.4}$ increases with the increase in the value of the coupling

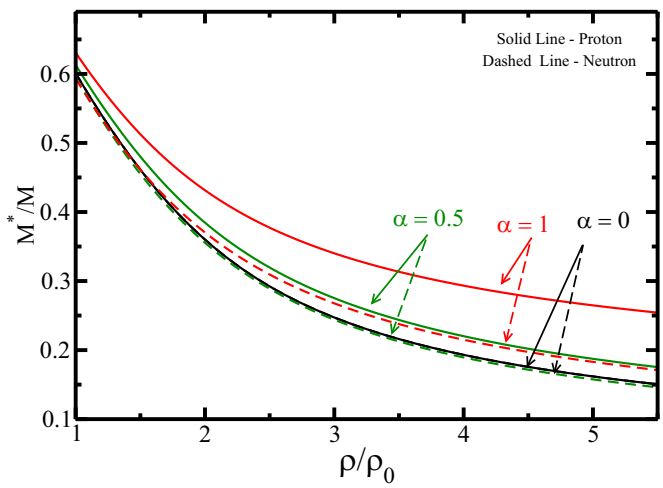

FIG. 4. Effective masses of proton and neutron for a few values of asymmetry parameter α for the SRV04 parametrization.

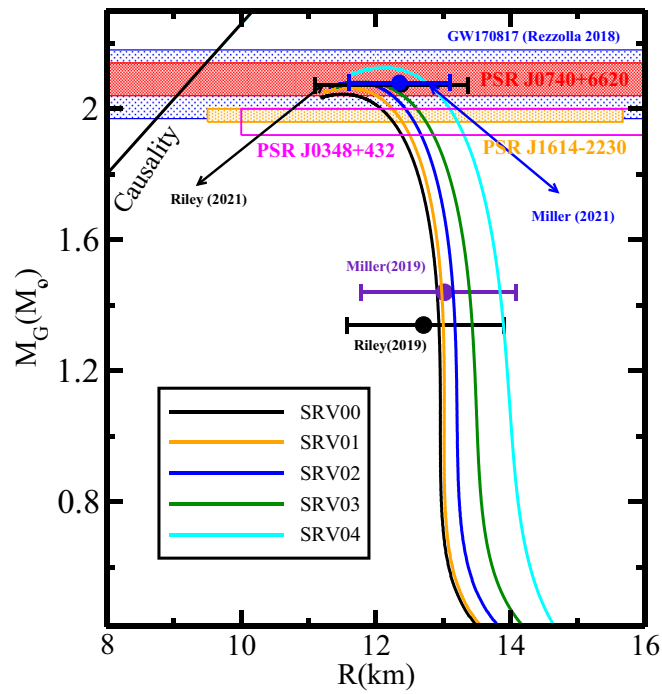

FIG. 5. Mass-radius relation of a neutron star for SRV parametrizations.

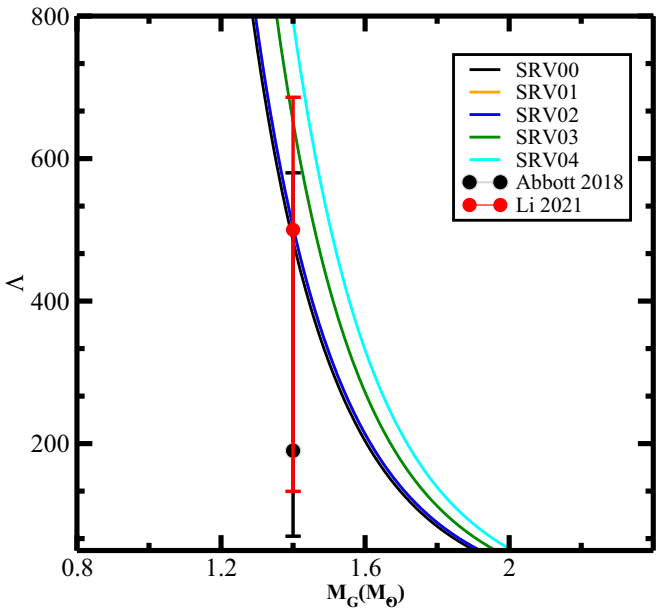

FIG. 6. Variation of dimensionless tidal deformability (Λ) with respect to gravitational mass for SRV parametrizations.

g_δ corresponding to the SRV parametrizations, as can be seen from Fig. 6. All these results are summarized in Table IV. The theoretical errors/uncertainties in neutron star properties for SRV parametrizations are also mentioned in the table. The neutron star properties such as $M_{\max}$, $R_{\max}$, $R_{1.4}$, $R_{2.0}$ are relatively well constrained for all SRV parametrizations (at $\leqslant 3\%$) whereas for $\Lambda_{1.4}$, the theoretical uncertainties are found to be $\leqslant 10\%$.

To this end, we may mention that the contribution of the δ meson is considered only through its linear interaction with nucleons. However, inclusion of the self-interaction of δ mesons and the mixed interactions with other mesons may alter the symmetry energy at suprasaturation densities. This would further enhance the flexibility of the EoS of dense matter and accordingly the properties of neutron stars [71–73]. Inclusion of the higher order contributions of the δ meson thus enables one to model the properties of neutron stars somewhat independently of the properties of finite nuclei. The optimization of the effective Lagrangian that includes different terms involving the δ meson field requires accurate knowledge of neutron star properties over a wide range of mass.

IV. SUMMARY AND CONCLUSIONS

The effect of the isovector scalar field corresponding to δ-meson in relativistic mean field theory is investigated. We have generated five sets of SRV parametrizations SRV00, SRV01, SRV02, SRV03, and SRV04 to explore the effects of the δ meson on the properties of finite nuclei, infinite nuclear matter, and neutron stars. A covariance analysis to measure the accuracy of model predictions is also performed. This also enabled us to carry out a systematic study of correlations among model parameters and various finite nuclei and infinite nuclear matter properties of interest. The SRV parametrizations have been obtained in such a way that they reproduce the ground state properties of the finite nuclei and infinite nuclear matter properties quite convincingly. In turn, they satisfy the constraints on mass and radius of the neutron star and its dimensionless tidal deformability, Λ, from recent astrophysical observations [8,66,67,78,81]. It is observed that to fit the properties of finite nuclei and infinite nuclear matter, a stronger coupling between the ρ meson and nucleons (g_ρ) is required in the presence of the δ meson field. Furthermore, the δ meson significantly affects the radius of a canonical neutron star. It is found that the contributions from the δ meson are important and have some significant effects on the dense matter EoS. The value of $\Lambda_{1.4}$ for different SRV parametrization is also in line with the constraint obtained from the GW170817 event. It is clear that the isovector splitting of the effective mass of nucleons in the presence of δ in dense asymmetric matter, like the scenario present in the core of a neutron star, can be significant. It remains, however, an open question how to identify in future the signatures of isovector effective mass splitting from astrophysical observations.

ACKNOWLEDGMENTS

V.T. is highly thankful to Himachal Pradesh University and DST-INSPIRE (Govt. of India) for providing computational facility and financial assistance (Junior/Senior Research Fellowship under Grant No. "DST/INSPIRE Fellowship/2017/IF170302"). C.M. acknowledges partial support from the IN2P3 Master Project "NewMAC".

[1] J. D. Walecka, A theory of highly condensed matter, Ann. Phys. (NY) **83**, 491 (1974).
[2] N. K. Glendenning and S. A. Moszkowski, Reconciliation of Neutron-Star Masses and Binding of the λ in Hypernuclei, Phys. Rev. Lett. **67**, 2414 (1991).
[3] M. Dutra, O. Lourenço, S. S. Avancini, B. V. Carlson, A. Delfino, D. P. Menezes, C. Providência, S. Typel, and J. R. Stone, Relativistic mean-field hadronic models under nuclear matter constraints, Phys. Rev. C **90**, 055203 (2014).
[4] M. Oertel, M. Hempel, T. Klähn, and S. Typel, Equations of state for supernovae and compact stars, Rev. Mod. Phys. **89**, 015007 (2017).
[5] X. Roca-Maza and N. Paar, Nuclear equation of state from ground and collective excited state properties of nuclei, Prog. Part. Nucl. Phys. **101**, 96 (2018).
[6] P. B. Demorest, T. Pennucci, S. M. Ransom, M. S. E. Roberts, and J. W. T. Hessels, A two-solar-mass neutron star measured using Shapiro delay, Nature (London) **467**, 1081 (2010).
[7] J. Antoniadis, P. C. C. Freire, N. Wex, T. M. Tauris, R. S. Lynch, M. H. van Kerkwijk, M. Kramer, C. Bassa, V. S. Dhillon, T.

Driebe *et al.*, A massive pulsar in a compact relativistic binary, Science **340**, 1233232 (2013).

[8] B. P. Abbott, R. Abbott, T. D. Abbott, F. Acernese, K. Ackley, C. Adams, T. Adams, P. Addesso, R. X. Adhikari, V. B. Adya *et al.*, GW170817: Measurements of Neutron Star Radii and Equation of State, Phys. Rev. Lett. **121**, 161101 (2018).

[9] B. P. Abbott, R Abbott, T. D. Abbott, F. Acernese, K. Ackley, C. Adams, T. Adams, P. Addesso, R. X. Adhikari, V. B. Adya *et al.*, Properties of the Binary Neutron Star Merger GW170817, Phys. Rev. X **9**, 011001 (2019).

[10] M. C. Miller, F. K. Lamb, A. J. Dittmann, S. Bogdanov, Z. Arzoumanian, K. C. Gendreau, S. Guillot, A. K. Harding, W. C. G. Ho, J. M. Lattimer, R. M. Ludlam, S. Mahmoodifar, S. M. Morsink, P. S. Ray, T. E. Strohmayer, K. S. Wood, T. Enoto, R. Foster, T. Okajima, G. Prigozhin *et al.*, PSR j0030+0451 mass and radius from NICER data and implications for the properties of neutron star matter, Astrophys. J. **887**, L24 (2019).

[11] T. E. Riley, A. L. Watts, S. Bogdanov, P. S. Ray, R. M. Ludlam, S. Guillot, Z. Arzoumanian, C. L. Baker, A. V. Bilous, D. Chakrabarty, K. C. Gendreau, A. K. Harding, W. C. G. Ho, J. M. Lattimer, S. M. Morsink, and T. E. Strohmayer, A NICER view of PSR j0030+0451: Millisecond pulsar parameter estimation, Astrophys. J. Lett. **887**, L21 (2019).

[12] M. C. Miller, F. K. Lamb, A. J. Dittmann, S. Bogdanov, Z. Arzoumanian, K. C. Gendreau, S. Guillot, W. C. G. Ho, J. M. Lattimer, M. Loewenstein *et al.*, The radius of PSR J0740+6620 from NICER and XMM-Newton data, Astrophys. J. Lett., **918**, L28 (2021).

[13] T. E. Riley, A. L. Watts, P. S. Ray, S. Bogdanov, S. Guillot, S. M. Morsink, A. V. Bilous, Z. Arzoumanian, D. Choudhury, J. S. Deneva *et al.*, A NICER view of the massive pulsar PSR J0740+6620 informed by radio timing and XMM-Newton spectroscopy, Astrophys. J. Lett. **918**, L27 (2021).

[14] J. M. Lattimer, Neutron stars and the nuclear matter equation of state, Annu. Rev. Nucl. Part. Sci. **71**, 433 (2021).

[15] D. Adhikari, H. Albataineh, D. Androic, K. Aniol, D. S. Armstrong, T. Averett, C. Ayerbe Gayoso, S. Barcus, V. Bellini, R. S. Beminiwattha *et al.*, Accurate Determination of the Neutron Skin Thickness of ^{208}Pb through Parity Violation in Electron Scattering, Phys. Rev. Lett. **126**, 172502 (2021).

[16] D. Adhikari *et al.* (CREX Collaboration), Precision determination of the neutral weak form factor of ^{48}Ca, Phys. Rev. Lett. **129**, 042501 (2022).

[17] R. Essick, I. Tews, P. Landry, and A. Schwenk, Astrophysical Constraints on the Symmetry Energy and the Neutron Skin of ^{208}Pb with Minimal Modeling Assumptions, Phys. Rev. Lett. **127**, 192701 (2021).

[18] P.-G. Reinhard, X. Roca-Maza, and W. Nazarewicz, Information Content of the Parity-Violating Asymmetry in ^{208}Pb, Phys. Rev. Lett. **127**, 232501 (2021).

[19] C. Mondal, Density dependence of symmetry energy and neutron skin thickness revisited using relativistic mean field models with nonlinear couplings, Phys. Rev. C **105**, 034305 (2022).

[20] P.-G. Reinhard, X. Roca-Maza, and W. Nazarewicz, Combined theoretical analysis of the parity-violating asymmetry for ^{48}Ca and ^{208}Pb, arXiv:2206.03134.

[21] E. Yüksel and N. Paar, Implications of parity-violating electron scattering experiments on ^{48}Ca (CREX) and ^{208}Pb (PREX-II) for nuclear energy density functionals, arXiv:2206.06527.

[22] B. D. Serot and J. D. Walecka, The relativistic nuclear many body problem, Adv. Nucl. Phys. **16**, 1 (1986).

[23] L.-W. Chen, C. M. Ko, and B.-A. Li, Isospin-dependent properties of asymmetric nuclear matter in relativistic mean field models, Phys. Rev. C **76**, 054316 (2007).

[24] M. Jaminon and C. Mahaux, Effective masses in relativistic approaches to the nucleon-nucleus mean field, Phys. Rev. C **40**, 354 (1989).

[25] X. Roca-Maza, M. Brenna, B. K. Agrawal, P. F. Bortignon, G. Colò, L.-G. Cao, N. Paar, and D. Vretenar, Giant quadrupole resonances in ^{208}Pb, the nuclear symmetry energy, and the neutron skin thickness, Phys. Rev. C **87**, 034301 (2013).

[26] X.-H. Li, W.-J. Guo, B.-A. Li, L.-W. Chen, F. J. Fattoyev, and W. G. Newton, Neutron-proton effective mass splitting in neutron-rich matter at normal density from analyzing nucleon-nucleus scattering data within an isospin dependent optical model, Phys. Lett. B **743**, 408 (2015).

[27] T. Malik, C. Mondal, B. K. Agrawal, J. N. De, and S. K. Samaddar, Nucleon effective mass and its isovector splitting, Phys. Rev. C **98**, 064316 (2018).

[28] T. Malik, B. K. Agrawal, J. N. De, S. K. Samaddar, C. Providência, C. Mondal, and T. K. Jha, Tides in merging neutron stars: Consistency of the GW170817 event with experimental data on finite nuclei, Phys. Rev. C **99**, 052801(R) (2019).

[29] S. Ghosh, D. Chatterjee, and J. Schaffner-Bielich, Imposing multi-physics constraints at different densities on the neutron star equation of state, Eur. Phys. J. A **58**, 37 (2022).

[30] P. J. Woods and C. N. Davids, Nuclei beyond the proton drip-line, Annu. Rev. Nucl. Part. Sci. **47**, 541 (1997).

[31] B.-A. Li, C. B. Das, S. Das Gupta, and C. Gale, Momentum dependence of the symmetry potential and nuclear reactions induced by neutron-rich nuclei at RIA, Phys. Rev. C **69**, 011603(R) (2004).

[32] J. Xu, L.-W. Chen, and B.-A. Li, Thermal properties of asymmetric nuclear matter with an improved isospin- and momentum-dependent interaction, Phys. Rev. C **91**, 014611 (2015).

[33] M. Baldo, G. F. Burgio, H.-J. Schulze, and G. Taranto, Nucleon effective masses within the Brueckner-Hartree-Fock theory: Impact on stellar neutrino emission, Phys. Rev. C **89**, 048801 (2014).

[34] W. Zuo, L. G. Cao, B. A. Li, U. Lombardo, and C. W. Shen, Isospin splitting of the nucleon mean field, Phys. Rev. C **72**, 014005 (2005).

[35] E. N. E. van Dalen, C. Fuchs, and A. Faessler, Effective Nucleon Masses in Symmetric and Asymmetric Nuclear Matter, Phys. Rev. Lett. **95**, 022302 (2005).

[36] D. Bandyopadhyay, C. Samanta, S. K. Samaddar, and J. N. De, Thermostatic properties of finite and infinite nuclear systems, Nucl. Phys. A **511**, 1 (1990).

[37] C. Mondal, B. K. Agrawal, J. N. De, S. K. Samaddar, M. Centelles, and X. Viñas, Interdependence of different symmetry energy elements, Phys. Rev. C **96**, 021302(R) (2017).

[38] C. Mondal, B. K. Agrawal, J. N. De, and S. K. Samaddar, Correlations among symmetry energy elements in Skyrme models, Int. J. Mod. Phys. E **27**, 1850078 (2018).

[39] Z. Zhang and L.-W. Chen, Isospin splitting of the nucleon effective mass from giant resonances in ^{208}Pb, Phys. Rev. C **93**, 034335 (2016).

[40] H.-Y. Kong, J. Xu, L.-W. Chen, B.-A. Li, and Y.-G. Ma, Constraining simultaneously nuclear symmetry energy and

neutron-proton effective mass splitting with nucleus giant resonances using a dynamical approach, Phys. Rev. C **95**, 034324 (2017).
[41] X. Roca-Maza, X. Viñas, M. Centelles, P. Ring, and P. Schuck, Erratum: Relativistic mean-field interaction with density-dependent meson-nucleon vertices based on microscopical calculations [Phys. Rev. C 84, 054309 (2011)], Phys. Rev. C **93**, 069905(E) (2016).
[42] S. Wang, H. F. Zhang, and J. M. Dong, Neutron star properties in density-dependent relativistic mean field theory with consideration of an isovector scalar meson, Phys. Rev. C **90**, 055801 (2014).
[43] V. Dexheimer, R. Negreiros, and S. Schramm, Reconciling nuclear and astrophysical constraints, Phys. Rev. C **92**, 012801(R) (2015).
[44] B. Kumar, S. K. Patra, and B. K. Agrawal, New relativistic effective interaction for finite nuclei, infinite nuclear matter, and neutron stars, Phys. Rev. C **97**, 045806 (2018).
[45] A. Kumar, H. C. Das, and S. K. Patra, Incompressibility and symmetry energy of a neutron star, Phys. Rev. C **104**, 055804 (2021).
[46] F. Li, B.-J. Cai, Y. Zhou, W.-Z. Jiang, and L.-W. Chen, Effects of isoscalar- and isoveclar meson mixing on neutron star structure, Astrophys. J. **929**, 183 (2022).
[47] S. K. Dhiman, R. Kumar, and B. K. Agrawal, Nonrotating and rotating neutron stars in the extended field theoretical model, Phys. Rev. C **76**, 045801 (2007).
[48] R. Kumar, B. K. Agrawal, and S. K. Dhiman, Effects of ω meson self-coupling on the properties of finite nuclei and neutron stars, Phys. Rev. C **74**, 034323 (2006).
[49] N. K. Glendenning, *Compact Stars: Nuclear Physics, Particle Physics, and General Relativity* (Springer-Verlag, New York, 2000).
[50] M. Wang, W. J. Huang, F. G. Kondev, G. Audi, and S. Naimi, The AME 2020 atomic mass evaluation (II). Tables, graphs and references, Chin. Phys. C **45**, 030003 (2021).
[51] I. Angeli and K. P. Marinova, Table of experimental nuclear ground state charge radii: An update, At. Data Nucl. Data Tables **99**, 69 (2013).
[52] P. Ring and P. Schuck, *The Nuclear Many-Body Problem* (Springer, New York, 1980).
[53] S. Karatzikos, A. V. Afanasjev, G. A. Lalazissis, and P. Ring, The fission barriers in actinides and superheavy nuclei in covariant density functional theory, Phys. Lett. B **689**, 72 (2010).
[54] T. Duguet, P. Bonche, P.-H. Heenen, and J. Meyer, Pairing correlations. II. Microscopic analysis of odd-even mass staggering in nuclei, Phys. Rev. C **65**, 014311 (2001).
[55] W.-C. Chen and J. Piekarewicz, Searching for isovector signatures in the neutron-rich oxygen and calcium isotopes, Phys. Lett. B **748**, 284 (2015).
[56] C. Mondal, B. K. Agrawal, J. N. De, and S. K. Samaddar, Sensitivity of elements of the symmetry energy of nuclear matter to the properties of neutron-rich systems, Phys. Rev. C **93**, 044328 (2016).
[57] B. K. Agrawal, S. Shlomo, and V. Kim Au, Determination of the parameters of a Skyrme type effective interaction using the simulated annealing approach, Phys. Rev. C **72**, 014310 (2005).
[58] T. J. Bürvenich, D. G. Madland, and P.-G. Reinhard, Adjustment studies in self-consistent relativistic mean-field models, Nucl. Phys. A **744**, 92 (2004).
[59] S. Kirkpatrick, Optimization by simulated annealing: Quantitative studies, J. Stat. Phys. **34**, 975 (1984).
[60] J. Dobaczewski, W. Nazarewicz, and P. G. Reinhard, Error estimates of theoretical models: A guide, J. Phys. G: Nucl. Part. Phys. **41**, 074001 (2014).
[61] C. Mondal, B. K. Agrawal, and J. N. De, Constraining the symmetry energy content of nuclear matter from nuclear masses: A covariance analysis, Phys. Rev. C **92**, 024302 (2015).
[62] S. Brandt, *Statistical and Computational Methods in Data Analysis* (Springer, New York, 1997).
[63] P.-G. Reinhard and W. Nazarewicz, Information content of a new observable: The case of the nuclear neutron skin, Phys. Rev. C **81**, 051303(R) (2010).
[64] F. J. Fattoyev, C. J. Horowitz, J. Piekarewicz, and Brendan Reed, GW190814: Impact of a 2.6 solar mass neutron star on the nucleonic equations of state, Phys. Rev. C **102**, 065805 (2020).
[65] P. Klüpfel, P.-G. Reinhard, T. J. Bürvenich, and J. A. Maruhn, Variations on a theme by Skyrme: A systematic study of adjustments of model parameters, Phys. Rev. C **79**, 034310 (2009).
[66] B.-A. Li and X. Han, Constraining the neutron–proton effective mass splitting using empirical constraints on the density dependence of nuclear symmetry energy around normal density, Phys. Lett. B **727**, 276 (2013).
[67] T.-G. Yue, L.-W. Chen, Z. Zhang, and Y. Zhou, Constraints on the symmetry energy from PREX-II in the multimessenger era, Phys. Rev. Res. **4**, L022054 (2022).
[68] G. Colo, U. Garg, and H. Sagawa, Symmetry energy from the nuclear collective motion: Constraints from dipole, quadrupole, monopole and spin-dipole resonances, Eur. Phys. J. A **50**, 26 (2014).
[69] J. Piekarewicz, Symmetry energy constraints from giant resonances: A relativistic mean-field theory overview, Eur. Phys. J. A **50**, 25 (2014).
[70] W.-C. Chen and J. Piekarewicz, Building relativistic mean field models for finite nuclei and neutron stars, Phys. Rev. C **90**, 044305 (2014).
[71] N. Zabari, S. Kubis, and W. Wójcik, Influence of the interactions of scalar mesons on the behavior of the symmetry energy, Phys. Rev. C **99**, 035209 (2019).
[72] N. Zabari, S. Kubis, and W. Wójcik, Anomalous quartic term in the expansion of the symmetry energy, Phys. Rev. C **100**, 015808 (2019).
[73] T. Miyatsu, M.-K. Cheoun, and K. Saito, Asymmetric nuclear matter in relativistic mean-field models with isoscalar-and isovector-meson mixing, Astrophys. J. **929**, 82 (2022).
[74] S. Kubis and M. Kutschera, Nuclear matter in relativistic mean field theory with isovector scalar meson, Phys. Lett. B **399**, 191 (1997).
[75] H. T. Cromartie, E. Fonseca, S. M. Ransom, P. B. Demorest, Z. Arzoumanian, H. Blumer, P. R. Brook, M. E. DeCesar, T. Dolch, J. A. Ellis *et al.*, Relativistic Shapiro delay measurements of an extremely massive millisecond pulsar, Nat. Astron. **4**, 72 (2020).
[76] E. Fonseca, H. T. Cromartie, T. T. Pennucci, P. S. Ray, A. Yu. Kirichenko, S. M. Ransom, P. B. Demorest, I. H. Stairs, Z. Arzoumanian, L. Guillemot *et al.*, Refined mass and geometric measurements of the high-mass PSR J0740+6620, Astrophys. J. Lett. **915**, L12 (2021).

[77] Y. Sugahara and H. Toki, Relativistic mean-field theory for unstable nuclei with non-linear σ and ω terms, Nucl. Phys. A **579**, 557 (1994).

[78] B. T. Reed, F. J. Fattoyev, C. J. Horowitz, and J. Piekarewicz, Implications of PREX-2 on the Equation of State of Neutron-Rich Matter, Phys. Rev. Lett. **126**, 172503 (2021).

[79] T. Hinderer, Tidal Love numbers of neutron stars, Astrophys. J. **677**, 1216 (2008).

[80] T. Hinderer, B. D. Lackey, R. N. Lang, and J. S. Read, Tidal deformability of neutron stars with realistic equations of state and their gravitational wave signatures in binary inspiral, Phys. Rev. D **81**, 123016 (2010).

[81] Y. Li, H. Chen, D. Wen, and J. Zhang, Constraining the nuclear symmetry energy and properties of the neutron star from GW170817 by Bayesian analysis, Eur. Phys. J. A **57**, 1 (2021).

[82] B. P. Abbott, R. Abbott, T. D. Abbott, F. Acernese, K. Ackley, C. Adams, T. Adams, P. Addesso, R. X. Adhikari, V. B. Adya *et al.* GW170817: Observation of Gravitational Waves from a Binary Neutron Star Inspiral, Phys. Rev. Lett. **119**, 161101 (2017).